Sixfold Increase in Historical Northern Hemisphere Concurrent Large Heatwaves Driven by Warming and Changing Atmospheric Circulations

CASSANDRA D. W. ROGERS,[a] KAI KORNHUBER,[b,c] SARAH E. PERKINS-KIRKPATRICK,[d,e] PAUL C. LOIKITH,[f] AND DEEPTI SINGH[a]

[a] *Washington State University, Vancouver, Washington*
[b] *Earth Institute, Columbia University, New York, New York*
[c] *Lamont-Doherty Earth Observatory, New York, New York*
[d] *University of New South Wales, Canberra, Australian Capital Territory, Australia*
[e] *ARC Centre of Excellence for Climate Extremes, Sydney, New South Wales, Australia*
[f] *Portland State University, Portland, Oregon*

(Manuscript received 16 March 2021, in final form 18 October 2021)

ABSTRACT: Simultaneous heatwaves affecting multiple regions (referred to as concurrent heatwaves) pose compounding threats to various natural and societal systems, including global food chains, emergency response systems, and reinsurance industries. While anthropogenic climate change is increasing heatwave risks across most regions, the interactions between warming and circulation changes that yield concurrent heatwaves remain understudied. Here, we quantify historical (1979–2019) trends in concurrent heatwaves during the warm season [May–September (MJJAS)] across the Northern Hemisphere mid- to high latitudes. We find a significant increase of ~46% in the mean spatial extent of concurrent heatwaves and ~17% increase in their maximum intensity, and an approximately sixfold increase in their frequency. Using self-organizing maps, we identify large-scale circulation patterns (300 hPa) associated with specific concurrent heatwave configurations across Northern Hemisphere regions. We show that observed changes in the frequency of specific circulation patterns preferentially increase the risk of concurrent heatwaves across particular regions. Patterns linking concurrent heatwaves across eastern North America, eastern and northern Europe, parts of Asia, and the Barents and Kara Seas show the largest increases in frequency (~5.9 additional days per decade). We also quantify the relative contributions of circulation pattern changes and warming to overall observed concurrent heatwave day frequency trends. While warming has a predominant and positive influence on increasing concurrent heatwave frequency, circulation pattern changes have a varying influence and account for up to 0.8 additional concurrent heatwave days per decade. Identifying regions with an elevated risk of concurrent heatwaves and understanding their drivers is indispensable for evaluating projected climate risks on interconnected societal systems and fostering regional preparedness in a changing climate.

SIGNIFICANCE STATEMENT: Heatwaves pose a major threat to human health, ecosystems, and human systems. Simultaneous heatwaves affecting multiple regions can exacerbate such threats. For example, multiple food-producing regions simultaneously undergoing heat-related crop damage could drive global food shortages. We assess recent changes in the occurrence of simultaneous large heatwaves. Such simultaneous heatwaves are 7 times more likely now than 40 years ago. They are also hotter and affect a larger area. Their increasing occurrence is mainly driven by warming baseline temperatures due to global heating, but changes in weather patterns contribute to disproportionate increases over parts of Europe, the eastern United States, and Asia. Better understanding the drivers of weather pattern changes is therefore important for understanding future concurrent heatwave characteristics and their impacts.

KEYWORDS: Atmosphere; Atmospheric circulation; Dynamics; Heating; Extreme events; Climate change; Temperature; Thermodynamics; Neural networks; Anomalies; Climate variability; Trends; Clustering

1. Introduction

Heatwaves, defined as high-temperature events that last for multiple consecutive days (Perkins et al. 2012), pose a major risk to human health (Hoegh-Guldberg et al. 2018; Xu et al. 2016), wildlife (e.g., McKechnie et al. 2012; Sharpe et al. 2019), and the natural and anthropogenic systems that societies depend on, including infrastructure (e.g., McEvoy et al. 2012) and agriculture (e.g., Kornhuber et al. 2020; van der Velde et al. 2010; Webb et al. 2010; Wehrli et al. 2020). For example, in August 2003, 40 000–70 000 deaths were attributed to a heatwave in Europe (World Meteorological Organization 2011). Heatwaves have become more frequent, longer lasting, and larger over the past few decades (Lyon et al. 2019; Perkins-Kirkpatrick and Lewis 2020; Vogel et al. 2020, 2019), with these trends expected to continue and accelerate due to unabated human emissions of greenhouse gases (Collins et al. 2013; Ganguly et al. 2009; Hoegh-Guldberg et al. 2018; Meehl and Tebaldi 2004; Seneviratne et al. 2012). However, changes in the characteristics of simultaneous heatwaves across multiple regions, here referred to as concurrent heatwaves, have not yet been investigated.

Supplemental information related to this paper is available at the Journals Online website: https://doi.org/10.1175/JCLI-D-21-0200.s1.

Corresponding author: Cassandra Rogers, cassandra.rogers@wsu.edu

DOI: 10.1175/JCLI-D-21-0200.1

Multiple extreme events occurring at the same time in remote regions can often result in more severe or compounding impacts than if the events were isolated (Raymond et al. 2020; Zscheischler et al. 2018). For example, simultaneous shocks from climate extremes to multiple agricultural regions have the potential to threaten global food supply (Gaupp et al. 2020; Kornhuber et al. 2020; Raymond et al. 2020; Tigchelaar et al. 2018). The reinsurance industry, which spreads financial risks across regions and sectors, is also vulnerable to compound extremes as increasing demand for payouts threatens profits (Raymond et al. 2020; Swiss Re 2019a,b). One such event occurred during the summer of 2018 where multiple locations including the British Isles, Siberia, and a number of European and eastern Asian countries, were affected by heat extremes simultaneously (Kornhuber et al. 2019; Vogel et al. 2019) leading to increased mortality, crop losses, infrastructure damage, and wildfires, among other impacts (Vogel et al. 2019). Examining such concurrent extremes together, which are occurring in a physically connected climate system, can provide important insights into their large-scale physical drivers and reduce the noise that might obscure their trends on regional scales.

Heatwaves in the midlatitudes are typically associated with regions of anomalously high pressure (anticyclones), which are often part of large-scale atmospheric waves (Perkins 2015; Petoukhov et al. 2016). Therefore, changes in midlatitude circulation patterns have the potential to alter heatwave characteristics (Horton et al. 2015). Observed increases in the occurrence of summer season heat extremes in the Northern Hemisphere have been related to an amplification (Petoukhov et al. 2016; Screen and Simmonds 2014) or increased frequency (Coumou et al. 2014; Lee et al. 2017; Mann et al. 2017) of high-amplitude, quasi-stationary wave patterns. Such patterns are projected to increase in frequency over the twenty-first century (Mann et al. 2018) and warm periods are likely to become more persistent, in part due to the weakening or slowdown of summertime storm tracks with enhanced warming (Kornhuber and Tamarin-Brodsky 2021; Pfleiderer et al. 2019).

Recent changes in summertime midlatitude circulation patterns have been linked to amplified warming at high latitudes, known as Arctic amplification (Coumou et al. 2018, 2015; Zhang et al. 2020). This amplified warming and the associated weakened meridional temperature gradient are associated with a weakening of the midlatitude summer storm tracks (Coumou et al. 2018, 2015), a weakening of fast-moving Rossby waves (Coumou et al. 2015), more persistent patterns (Coumou et al. 2014), and an amplification (Coumou et al. 2018) or increase in the frequency of quasi-stationary waves (Coumou et al. 2014) in summer. Zhang et al. (2020) also find that reductions in Arctic sea ice and snow cover in Eurasia drive changes in midlatitude circulation and heatwaves in Europe, and Wu and Francis (2019) find that an increased frequency of low pressure systems during the Arctic summer can influence the development of East Asian heatwaves. While the attribution of historical changes in atmospheric circulation to anthropogenic warming and the role of Arctic amplification is still uncertain (Barnes and Screen 2015; Cohen et al. 2020; Francis 2017), these findings underline the importance of understanding dynamical (circulation) changes and teleconnections between circulation patterns and heatwaves in multiple locations in the Northern Hemisphere.

As well as influencing regional heat extremes, circumglobal teleconnections and Rossby waves are linked to the co-occurrence of heat extremes in the Northern Hemisphere. Röthlisberger et al. (2019) find that synoptic-scale recurrent Rossby waves resulted in simultaneous warm spells over Europe, North America, and the western North Atlantic in the summer of 1994. Similarly, Kornhuber et al. (2020) find that specific Rossby wave configurations are associated with concurrent heatwaves in central North America, eastern Europe, and eastern Asia (wavenumber 5), and central North America, western Europe, and western Asia (wavenumber 7). Ding and Wang (2005) similarly note a relationship between anomalous air temperatures in the Northern Hemisphere summer and circumglobal teleconnections. Changes in concurrent heatwaves can therefore be associated with warming (thermodynamics) and changes in circulation patterns (dynamics), although their influence on historical trends in concurrent heatwaves has not been studied. While the contribution of circulation changes to heat extremes is quite noisy at regional scales (e.g., Horton et al. 2015), previous studies have found significant changes in quasi-resonant, large-scale atmospheric patterns that favor heat extremes across multiple midlatitude regions (Coumou et al. 2014; Mann et al. 2017). These studies highlight the potential for dynamics to influence the location, trends, and characteristics of concurrent heatwaves.

Here, we quantify overall historical trends in Northern Hemisphere concurrent heatwave characteristics, identify their physical drivers, and investigate to what extent changes in atmospheric circulation patterns have increased the risk of concurrent heatwaves. Specifically, we address three main questions: 1) How has the frequency, intensity, and extent of large concurrent heatwaves changed between 1979 and 2019? 2) Which regions have the highest risk of experiencing concurrent heatwaves associated with different circulation patterns? And 3) how have recent dynamic (circulation) and thermodynamic (warming) changes contributed to the observed changes in concurrent heatwave characteristics?

Our study makes novel contributions to the literature by quantifying understudied yet societally relevant characteristics of heatwaves and studying the drivers of physically connected heatwaves. While previous research has linked concurrent heatwaves in specific regions to specific rare circulation patterns (Kornhuber et al. 2020, 2019; Pfahl and Wernli 2012; Röthlisberger et al. 2019), our paper introduces a methodology that can objectively classify all configurations of concurrent heatwaves that occur anywhere in our study region and link them to different atmospheric patterns, thereby capturing a wider range of potentially high-impact events. A thorough understanding of the drivers of concurrent heat extremes is important for climate model validation, assessing the sources of uncertainties, and improving the reliability of future model projections of concurrent weather extremes in the Northern Hemisphere. Further, identifying the regions at risk of experiencing such events can help predict their societal impacts on globally connected systems and can assist in preparation for these events by focusing adaptation and mitigation efforts in these regions.

2. Data

We utilize the ERA5 reanalysis data (Hersbach et al. 2019), which are produced by the European Centre for Medium-Range Weather Forecasts (ECMWF). Hourly data are available on a 0.25° × 0.25° grid (Copernicus Climate Change Service 2021a,b). We use ERA5 hourly 2-m maximum and minimum temperature data (Hennermann 2020) from 1979 to 2019 to produce daily mean temperature data for characterizing concurrent heatwaves. We calculate daily maximum (minimum) temperature from the hourly data as the maximum (minimum) of the hourly maximum (minimum) temperature for that day—that is, from 0000 UTC on day x to 2300 UTC on day x, inclusive. Daily mean temperature data are calculated as the average of the daily maximum and minimum temperatures for any given day. We use this temperature metric due to its correlation with health impacts (Nairn and Fawcett 2015; Nicholls et al. 2008) and usage for operational purposes (Australian Bureau of Meteorology 2020). We use ERA5 daily average 300-hPa geopotential height data to identify characteristic circulation patterns in the extended summer season [May–September (MJJAS)]. Surface temperatures in the midlatitudes are generally closely related to upper-tropospheric geopotential heights. Geopotential heights are widely used in meteorology to track pressure systems, including high pressure systems that are typically associated with heatwaves at the surface, as they drive adiabatic descent and warming. Numerous studies have used 500-hPa geopotential heights to study the relationship between atmospheric circulations and near-surface extremes (e.g., Cattiaux et al. 2016; Horton et al. 2015; Loikith and Broccoli 2012; Singh et al. 2016). Further, sea level pressure, which helps explain advection, is not a primary driver of summer heat in the midlatitudes and thus is not an ideal metric for examining summer temperature extremes. Therefore, we use upper-level geopotential heights, rather than sea level pressure, to capture the large-scale atmospheric circulation patterns that we expect are associated with concurrent heatwaves, and to avoid noise in sea level pressure data that might arise due to topography complexity or surface inhomogeneities (Loikith and Broccoli 2012).

3. Methods

a. Heatwave definitions

We define heatwaves as a period of three or more consecutive days with daily mean temperature at 2 m greater than the local 90th percentile, similar to Nairn and Fawcett (2015) and Rogers et al. (2019). We use a seasonally varying heatwave threshold at each grid cell, where the threshold for each day in MJJAS is calculated as the 90th percentile of daily mean temperature values for the given day between 1981 and 2010. We use the 1981–2010 climatology for consistency with the last World Meteorological Organization climate normal period (World Meteorological Organization 2021). These data are then smoothed using a 31-day moving window to remove noise. This temporally moving threshold accounts for the seasonal cycle of temperature, meaning that heatwaves can be identified in all months (MJJAS), rather than preferentially occurring around the hottest part of the year. The percentile thresholds account for spatial variations in the temperature climatology. A single heatwave consists of all connected grid cells under heatwave conditions at the same time, where grid cells are considered connected if they have a common edge. *Heatwave extent* is defined as the sum of the area of all connected grid cells under heatwave conditions on the same day. *Heatwave intensity* is defined as the area-weighted average standardized daily mean temperature anomaly (relative to the local 1981–2010 mean) across all connected grid points within the large heatwave.

b. Concurrent heatwave metrics

We define *concurrent heatwave days* as any day with two or more individual large heatwaves occurring anywhere within the study region (20°–80°N). A sample concurrent heatwave day is shown in Fig. 1 to illustrate how we identify these events. *Concurrent heatwave intensity* is defined as the average intensity of all heatwaves that occur on a concurrent heatwave day. The seasonal maximum (mean) concurrent heatwave intensity is calculated as the maximum (mean) intensity of all concurrent heatwave days within the season. Similarly, we define *concurrent heatwave extent* as the average extent of all heatwaves that occur on a concurrent heatwave day and then determine the seasonal maximum and mean concurrent heatwave extent. Comparing the seasonal maximum and seasonal mean intensity (or extent) allows us to understand whether the most intense (or widespread) concurrent heatwave events are changing at a different rate than the moderate events.

We restrict our analysis to large heatwaves with an extent exceeding ~1 600 000 km^2 (approximately the size of Mongolia or Iran), corresponding to the 98th percentile of heatwave extent for all heatwaves larger than one grid cell. We use the large heatwave threshold to focus on the most widespread events that affect a large number of people or large regions, which have the potential for generating severe societal impacts as witnessed in recent summer seasons. We test the sensitivity of our results to our threshold choice (Fig. S1 in the online supplemental material) by varying the threshold from the 95th (~600 000 km^2) to the 99th (~2 500 000 km^2) percentile. The use of a lower percentile threshold (95th–97th percentile) results in the identification of concurrent heatwaves every day for multiple years at the end of the time series, making the trends unclear (Fig. S1a). Using the 98th percentile heatwave extent threshold allows for a sufficient sample size to robustly evaluate changes in concurrent large heatwaves over the observed record. While heatwave extent is understudied in the literature, a small number of papers also use minimum heatwave extent thresholds to limit their studies to large heatwaves, such as Rebetez et al. (2009), who calculate the extent of June 2003 heatwaves over Europe to be ~1 600 000 km^2, and Lyon et al. (2019), who examine concurrent heatwaves over the contiguous United States using an extent threshold of ~151 000 km^2. Further, the overall observed trends in concurrent heatwave characteristics remain largely insensitive to the selected extent threshold (Fig. S1).

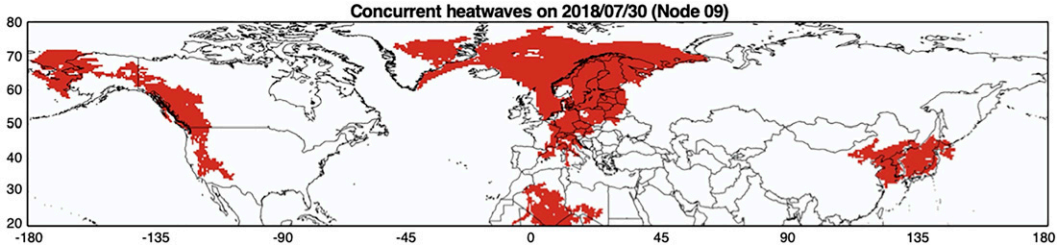

FIG. 1. Heatwave locations on 30 Jul 2018. Red pixels indicate grid cells that were under heatwave conditions on 30 Jul 2018. Four heatwaves occurred on this day, with a minimum extent of 2 100 000 km^2, a maximum extent of 7 500 000 km^2, and a mean extent of 3 800 000 km^2. Mean heatwave intensity on this day is ~2.0 standard deviations (σ) above the mean. This day occurs under a geopotential height pattern best matched to node 9 in Fig. 4.

While we characterize several concurrent heatwave metrics, one limitation of our methods is the inability to determine concurrent heatwave duration since large heatwaves might significantly change location over a number of days, merge with other heatwaves, or split into multiple heatwaves. Therefore, rather than examining the number or duration of multiday heatwave events, we examine the number of concurrent heatwave days in MJJAS.

c. *Characterization of circulation patterns using self-organizing maps*

Different atmospheric circulation patterns can cause concurrent heatwaves across different regions in the Northern Hemisphere (e.g., Kornhuber et al. 2020). We use self-organizing maps (SOMs) to identify typical atmospheric patterns (e.g., Gibson et al. 2016; Jiang et al. 2015, 2012; Thomas et al. 2021) that occur over the midlatitudes and characterize concurrent heatwaves associated with each pattern. A SOM is an unsupervised clustering algorithm that uses iterative statistical processes to identify representative patterns, referred to as clusters or nodes, in a high-dimensional dataset (Kohonen 2014). It does not require a priori knowledge of specific patterns or configurations. SOMs yield a continuum of patterns without the constraint of orthogonality such as with principal component analysis and each SOM node pattern is a composite of the underlying, relatively similar patterns in each cluster.

We use the SOM Toolbox Matlab package, developed by the Helsinki University of Technology (Laboratory of Computer and Information Science 2009), to apply SOMs to daily 300-hPa geopotential height anomalies from ERA5 reanalysis to classify daily atmospheric patterns over the midlatitudes (30°–60°N). The use of a narrow latitude band to train the SOM ensures that we are only considering midlatitude circulation features when creating the SOM and any variability outside this region does not affect the creation of the SOM; thus, the identified circulation patterns show the most frequently occurring geopotential height features in the midlatitudes. We use a 3 × 4 SOM configuration to identify the circulation patterns. After testing several different map sizes (not shown), we find that the 3 × 4 SOM has a sufficient number of circulation patterns to capture the diversity of the underlying patterns without creating duplicate patterns. We use batch training (Jiang et al. 2015, 2012; Kohonen 2014), the Epanechikov neighborhood function (Liu et al. 2006), random initialization, and training radii of 5–1 and 2–1 to produce our SOM. The SOM is trained using two rounds of training with coarse and fine training lengths of 1000 and 4000, respectively, where training length refers to the number of times that the entire dataset is presented to the SOM for training. Prior to choosing these SOM parameters, we performed a number of tests to ensure that our SOM is accurate and stable, whereby the nodes are a good representation of the data used to train the SOM and are insensitive to small changes in various SOM parameters. A detailed description of the SOM and our parameter selection is provided in section S2 of the online supplemental material. Further details of the SOM Toolbox Matlab package are provided in Kohonen (2014) and Vesanto et al. (2000).

Geopotential height anomalies are calculated by subtracting the climatological average daily geopotential height from the daily geopotential height to remove the seasonal cycle. The daily climatological average is calculated over 1981–2010 at each grid cell using a 31-day moving window. We apply an additional smoothing to the geopotential height anomalies using a 3-day running mean to reduce variability shorter than the duration of a heatwave. Geopotential height data are also area-weighted by multiplying data by the square root of the cosine of the latitude to ensure that data at all latitudes influence the SOM equally. Due to computational limitations, we regrid the 0.25° × 0.25° geopotential height and temperature data onto a 0.5° × 0.5° grid using bilinear interpolation prior to creating the SOM.

d. *Concurrent heatwaves and SOM analysis*

To examine the patterns of concurrent heatwaves associated with the typical atmospheric patterns, we identify concurrent heatwaves on all days associated with each node. We use a larger study region (20°–80°N) than is used to create the SOM (30°–60°N) to allow for possible teleconnections between midlatitude circulation patterns and mid- to high-latitude concurrent heatwaves. The concurrent heatwave day frequency for node i is calculated as the total number of concurrent heatwave days that are associated with node i each MJJAS season. We examine the number of concurrent heatwave days per node per season to examine how changes in circulation patterns influence changes in concurrent heatwave days. This metric is used to calculate the results in Table 1.

TABLE 1. Trends decomposed by SOM node. Trends in the number of node occurrences per season (second column) and the number of concurrent heatwave days per season (third column), also referred to as the total contribution in Fig. 7. The bold italic font in columns 1–3 indicates trends that are significant using the Mann–Kendall test at the 95% confidence level. The "+" and "−" symbols in the first column indicate nodes that have increased or decreased significantly over time, respectively. The fourth column shows the portion of the trend in the number of concurrent heatwave days that is due to thermodynamics, the fifth column shows the portion due to dynamics, and the sixth column shows the portion due to the interactive term. The sum of the thermodynamic, dynamic, and interactive terms (columns 4–6) is equal to the total contribution (column 3). The last column is the dynamic term as a percentage of the thermodynamic term.

SOM node	Trend in node occurrence (days per season)	Trend in concurrent heatwave days per season	Thermodynamic contribution	Dynamic component	Interactive component	Percentage (%)
1	−0.10	***0.28***	0.26	−0.05	0.06	−17.4
2	0.19	***0.36***	0.27	0.10	−0.02	36.9
3	−0.08	***0.26***	0.32	−0.04	−0.02	−13.3
4	0.11	***0.39***	0.33	0.06	0.00	18.1
***5* (+)**	***0.59***	***0.70***	0.32	0.30	0.08	93.6
6	0.07	***0.33***	0.33	0.03	−0.03	10.2
7	−0.30	***0.19***	0.33	−0.15	0.01	−44.5
8	0.19	***0.39***	0.31	0.10	−0.02	32.6
***9* (+)**	***0.23***	***0.52***	0.35	0.13	0.04	36.1
***10* (−)**	***−0.43***	***0.13***	0.37	−0.21	−0.03	−57.8
***11* (−)**	***−0.22***	***0.16***	0.26	−0.11	0.01	−41.4
***12* (−)**	***−0.25***	***0.18***	0.26	−0.12	0.04	−46.8

To determine *hotspots* of concurrent heatwave occurrence for each node (Fig. 5), we examine the number of large concurrent heatwaves that each grid cell is involved in and quantify their significance. The significance of concurrent heatwave frequencies for each node is determined using a Monte Carlo simulation by comparing the actual frequencies to data that are randomly sampled from all nodes. For example, if node j occurs n times, we randomly sample n days from the total dataset and calculate the concurrent heatwave frequency for each grid box. After repeating this process m times ($m = 500$) we calculate the 90th percentile of the number of large concurrent heatwaves over each grid box to use as thresholds. If the actual concurrent heatwave frequency for a given grid cell for node j is greater than the local 90th percentile threshold, the grid box is significantly more likely to experience concurrent heatwaves when under the influence of node j than is expected due to chance. If all nodes occurred equally, each node would occur 8.3% of the time. To ensure that the concurrent heatwave frequencies are not biased by how often the node occurs, we standardize the percentage of occurrence by multiplying the results by 8.3% and dividing by the actual node frequency (as a percentage).

e. *Thermodynamic (warming driven) versus dynamic (circulation driven) contributions*

To determine the drivers of historical trends (1979–2019) in the number of concurrent heatwave days, we isolate the contribution of mean warming and changes in circulation patterns. Following Cassano et al. (2007) and Horton et al. (2015), the trend in the frequency of concurrent heatwave days can be expressed as

$$H = \sum_{i=1}^{n} H_i f_i, \tag{1}$$

where H is the time series of the number of concurrent heatwave days within MJJAS of each year over the 20°–80°N study region for all nodes, H_i is the number of concurrent heatwave days for node i divided by the number of days that node occurs (referred to as the fraction of concurrent heatwave days), f_i is the number of days that node i occurs (referred to as node frequency), and n is the number of nodes in the SOM ($n = 12$).

This can be expanded as follows:

$$H = \sum_{i=1}^{n} (\overline{H}_i + H_i')\left(\overline{f}_i + f_i'\right), \tag{2}$$

where $\overline{H}_i$ is the mean fraction of node i occurrences that are concurrent heatwave days, and H_i' is the time series of deviations from $\overline{H}_i$. Similarly, $\overline{f}_i$ is the mean frequency of node i, and f_i' is the time series of deviations from $\overline{f}_i$.

The derivative of these terms can be expressed as follows:

$$\frac{d}{dt}H = \sum_{i=1}^{n}\left(\overline{f}_i \frac{d}{dt} H_i' + \overline{H}_i \frac{d}{dt} f_i' + \frac{d}{dt} H_i' f_i'\right), \tag{3}$$

where dH/dt is the overall seasonal trend in the number of concurrent heatwave days in MJJAS (1979–2019) across all nodes, dH_i'/dt is the seasonal trend in the fraction of node i occurrences that are concurrent heatwave days, df_i'/dt is the seasonal trend in the frequency of node i, and $dH_i'f_i'/dt$ is the trend in the product of the annual deviations from $\overline{H}_i$ and $\overline{f}_i$. The three terms on the right side of Eq. (3), from left to right, can be interpreted as follows:

(i) *Thermodynamic contribution* $\overline{f}_i dH_i'/dt$: The thermodynamic, or warming-driven, term is defined as the product of the mean frequency of node i and the trend in the

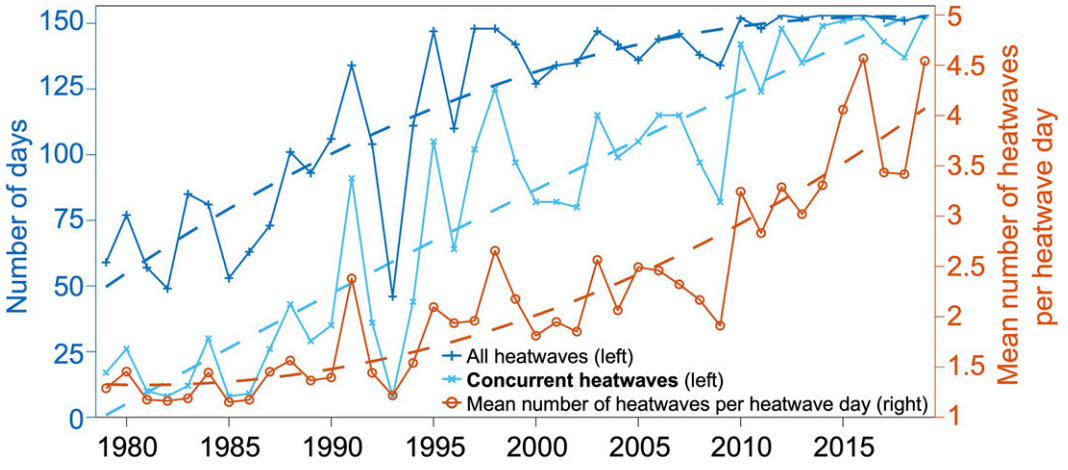

FIG. 2. Northern Hemisphere heatwave characteristics. Time series of the frequency of heatwave days (solid dark blue line with "+" markers; left axis), concurrent heatwave days (solid light blue line with "×" markers; left axis), and the mean number of heatwaves per heatwave day per MJJAS season (solid orange line with "o" markers; right axis). Heatwave days are defined as the number of days per MJJAS season with one or more heatwaves. Concurrent heatwave days are defined as the number of days per MJJAS season with two or more heatwaves. Dashed trend lines are either linear or quadratic depending on which line fits the data best. All trends are significant at the 95% confidence level based on the Mann–Kendall test (Fatichi 2020).

fraction of node i occurrences that are concurrent heatwave days. This term is the portion of the trend in the number of concurrent heatwave days that is solely due to changes in temperature assuming no changes in frequency of circulation patterns.

(ii) *Dynamic contribution* $\overline{H}_i df_i'/dt$: The dynamic, or circulation-driven, term is defined as the product of the mean fraction of node i days that are concurrent heatwave days and the trend in the frequency of node i. This term is the portion of the trend in the number of concurrent heatwave days that is due solely to changes in circulation patterns assuming that the fraction of concurrent heatwaves associated with each pattern occurrence remains unchanged.

(iii) *Interactive term contribution* $dH_i' f_i'/dt$: The interactive term is the trend in the product of the deviations from the mean of the fraction of node i occurrences that are concurrent heatwave days and the frequency of the node occurrence. This interactive term represents interactions between the dynamic and thermodynamic components, such as feedbacks between near-surface temperature and atmospheric patterns through soil moisture interactions.

This methodology is used to assess the dynamic, thermodynamic, and interactive term contributions from each node to the overall trend in concurrent heatwaves using upper-level geopotential height to represent circulation patterns. This method for decomposing trends has been widely implemented to examine trends in precipitation (Cassano et al. 2007; Tan et al. 2019a; Zhou et al. 2020), extreme precipitation (Tan et al. 2019b; Yu et al. 2018), temperature (Tan et al. 2019a), extreme temperature (Gao et al. 2019; Horton et al. 2015; Sui et al. 2020), and meltwater (Mioduszewski et al. 2016). We also quantify the contributions of the various mechanisms to the concurrent heatwave trends at each grid cell to examine variations in their relative contributions across regions. For this, we create a time series of the number of days at each grid point that are part of a large concurrent heatwave event. The total thermodynamic, dynamic, and interactive term contributions from all nodes are then evaluated for this time series.

4. Results and discussion

a. Trends in concurrent heatwave characteristics

Multiple studies show that local and regional heatwaves have increased in duration, frequency, and intensity over time (e.g., Meehl and Tebaldi 2004; Perkins-Kirkpatrick and Lewis 2020; Perkins et al. 2012). However, the drivers of and spatiotemporal trends in concurrent heatwaves in the Northern Hemisphere have not yet been investigated. We find that while the average number of MJJAS days with at least one large heatwave doubled from the 1980s (~73) to the 2010s (~152; Fig. 2), the number of concurrent heatwave days increased from an average of ~20 days per season in the 1980s to ~143 days per season in the 2010s, an approximately sixfold increase. Here, the number of concurrent heatwave days is defined as the number of days with two or more co-occurring heatwaves larger than ~1 600 000 km^2 in the mid- to high latitudes (20°–80°N). This amounts to concurrent heatwaves occurring nearly every day within the 153 days of the Northern Hemisphere warm season by 2019. The increase in the number of concurrent heatwave days is associated with a nonlinear increase in the number of heatwaves occurring per heatwave day, with an average of 1.3 heatwaves per heatwave day in the 1980s to an average of 3.6 per heatwave day in the 2010s (Fig. 2). In the MJJAS seasons of 2016 and 2019, two of the hottest years on record (NASA 2020), the average number of heatwaves exceeded 4.5 heatwaves per heatwave day. Therefore, concurrent heatwave days have become more frequent and

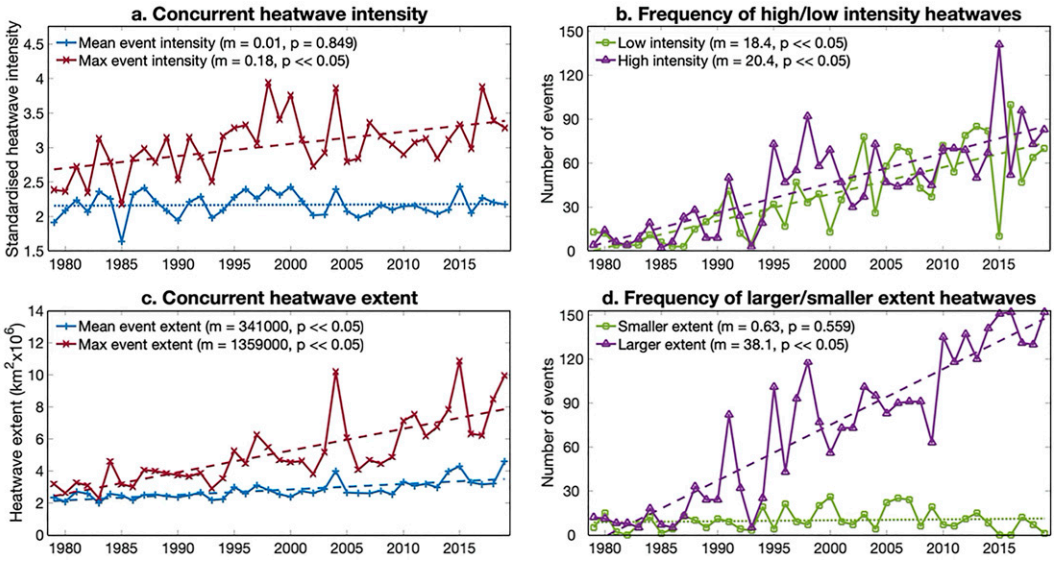

FIG. 3. Changes in concurrent heatwave intensity and extent over time. Time series of (a) mean concurrent heatwave intensity (solid blue line with "+" markers) and maximum concurrent heatwave intensity (solid red line with "×" markers), (b) the number of concurrent heatwave events with an intensity below the median intensity (solid green line with square markers), and above or equal to the median (solid purple line with triangle markers), where the median intensity is calculated using a base period of 1981–2010. (c),(d) As in (a) and (b), but for concurrent heatwave extent. Values in parentheses in the legends give the change in each time series per decade (m) and the p value. Dashed (dotted) lines show significant (nonsignificant) linear trends. Trend significance is determined using the Mann–Kendall test (Fatichi 2020) at the 95% confidence level.

more heatwaves are occurring on each of these days. These results demonstrate that there is an increasing risk of multiple regions simultaneously experiencing heatwaves.

We also find substantial changes in the mean intensity and contiguous extent of concurrent heatwaves. In Fig. 3a we find that the hottest concurrent heatwaves have become hotter over time, as indicated by the significant positive trend in the seasonal maximum intensity. The seasonal maximum concurrent heatwave intensity increased by ~17%, from 2.7 standard deviations (σ) above the seasonal mean in the 1980s to 3.2σ in the 2010s, even though the seasonal mean intensity remained unchanged (Fig. 3a). These trends can be explained by similar trends in the number of high-intensity (≥median intensity) and low-intensity (<median intensity) concurrent heatwave events, which increased significantly by 20.4 and 18.4 events per decade, respectively (Fig. 3b). The occurrence of relatively similar trends in the number of high- and low-intensity concurrent heatwaves (Fig. 3b) explains the lack of significant change in mean concurrent heatwave intensity (Fig. 3a). While the lack of trend in mean concurrent heatwave intensity might seem to suggest that the severity of heatwaves has not changed over time, these results indicate that the mid- to high latitudes are exposed to increased risk from high-intensity concurrent events, consistent with Perkins-Kirkpatrick and Lewis (2020), who did not find widespread increases in mean heatwave intensity over land areas but did find an increase in the cumulative intensity by these events due to increased duration.

In contrast to the intensity trends, we find that both the seasonal mean and maximum concurrent heatwave extent have significantly increased over the 41 years (Fig. 3c). The increase is more pronounced for maximum average concurrent heatwave extent, which increased by 1 400 000 km^2 per decade, up to an average of 7 700 000 km^2 (approximately the size of Australia) in the 2010s (Fig. 3c), which is an increase of ~130%. Mean heatwave extent also increased significantly but at approximately one-quarter of the rate of seasonal maximum increase (~340 000 km^2 per decade, ~46% increase). We further investigate trends in the number of days with larger and smaller concurrent heatwave extent, where smaller (larger) extent events are less than (greater than or equal to) the median extent of concurrent heatwave events calculated across 1981–2010. While the number of smaller extent events did not show a significant change over time, the number of larger extent events increased significantly from an average of ~13 events per season in the 1980s to ~137 events per season in the 2010s (an increase of ~38 days per decade). Since this trend in the number of larger extent heatwaves could in part be due to background temperature increases resulting in two smaller heatwaves merging into one larger one, this further emphasizes the strength of the trend in the number of heatwaves per heatwave day (Fig. 2). Similarly, Vogel et al. (2019) noted an increase in the land area simultaneously under heatwave conditions since 1958. They conclude that the unprecedented extent of events in recent years could not have occurred in the absence of global warming.

b. *Concurrent heatwaves and associated large-scale atmospheric circulation patterns*

Global mean warming, driven largely by an increase in anthropogenic activities, has contributed to an increase in the

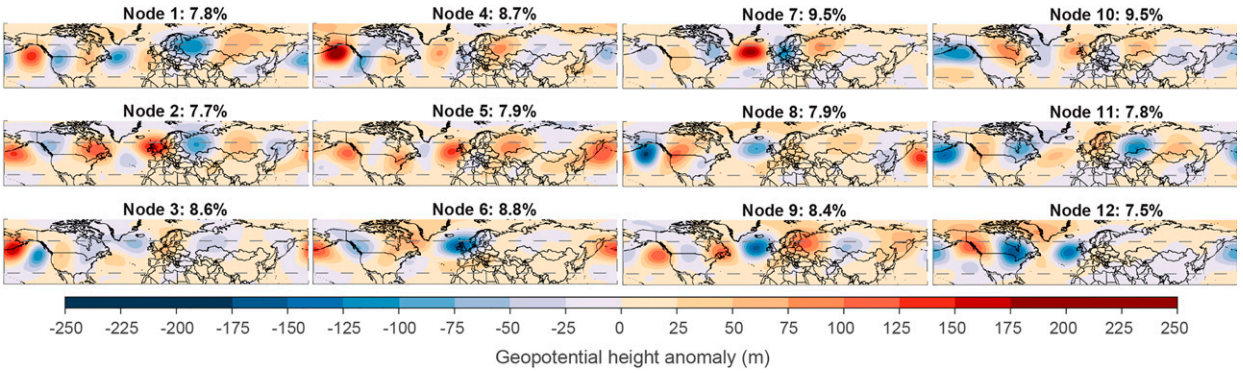

FIG. 4. Characteristic circulation patterns, with a 3 × 4 SOM showing anomalous geopotential height anomaly patterns at 300 hPa between 1979 and 2019, for MJJAS only. The dashed box shows the region used to define the nodes. Percentages above each subplot show how frequently each node occurs. Note that the color bar is not linear at the tails.

number of heatwaves across much of the world (IPCC 2013; Perkins 2015), with trends in atmospheric circulations contributing to an increase in the number of heatwaves in some regions (Horton et al. 2015). Given the role of large-scale atmospheric circulations in driving concurrent heatwaves in multiple regions, we examine whether there are detectable changes in circulation patterns associated with concurrent heatwaves and whether those trends affect the frequency and location of concurrent heatwaves.

The 12 characteristic circulation patterns (nodes) identified using our SOM (Fig. 4) show wavelike features with meridionally alternating regions of high and low 300-hPa geopotential height anomalies across the Northern Hemisphere midlatitudes. Concurrent heatwave hotspots (Fig. 5) are closely related to the location of positive geopotential height anomalies associated with each large-scale circulation pattern (Fig. 4). Nonstippled areas in Fig. 5, referred to as hotspots, indicate regions where concurrent heatwaves occur more frequently than can be expected due to chance during the occurrence of the associated geopotential height pattern. For example, node 5 (Fig. 4) is associated with high geopotential heights over the northeast Pacific, the northwest Pacific, the eastern United States, the eastern Atlantic, and western Russia, and has concurrent heatwave hotspots (Fig. 5; node 5) over the northeast Pacific, the northwest Pacific and eastern Asia, the eastern United States, the North Atlantic, western Asia, the Barents and Kara Seas, and northeastern Africa. Therefore, these hotspot regions were more likely to have been under concurrent heatwave conditions when an atmospheric circulation resembling the node 5 pattern was present (Fig. 4). Similarly, hotspots associated with the other nodes (Fig. 5) tend to be collocated or occur slightly to the west of the regions of anomalously high geopotential heights (Fig. 4), likely associated with the advection of relatively warm air northward from the lower latitudes.

We note that the hotspots do not always experience heatwaves at the same time. For example, Fig. 1 shows that on 30 July 2018 (a node 9 day), a large heatwave occurred over northern Europe, Scandinavia, and the surrounding Arctic Ocean, which aligns with one of the hotspots in node 9. However, two of the other hotspots, northeastern North America and eastern Russia, were not under heatwave conditions on this day. Although the SOM patterns are determined using data in the midlatitudes only (30°–60°N), we find that hotspots

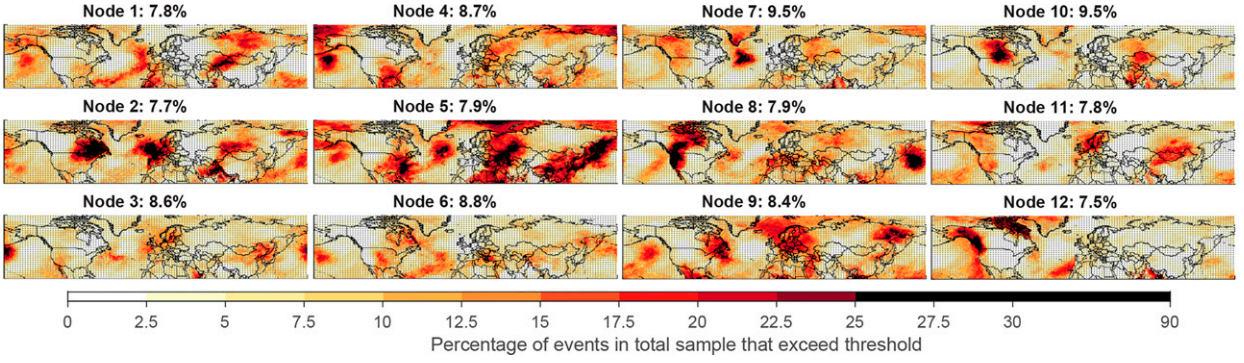

FIG. 5. Concurrent heatwave frequency maps. Maps showing the percentage of large concurrent heatwaves that occur in a given node normalized by the frequency of occurrence of the corresponding node. Stippling shows where the percentage of concurrent heatwaves in that node is not significantly greater than if the data are randomly sampled. Significance is determined using the Mann–Kendall test (Fatichi 2020) at the 95% confidence level. Percentages above each subplot show how frequently each node occurs. Note that the color bar scale is not linear above 25.

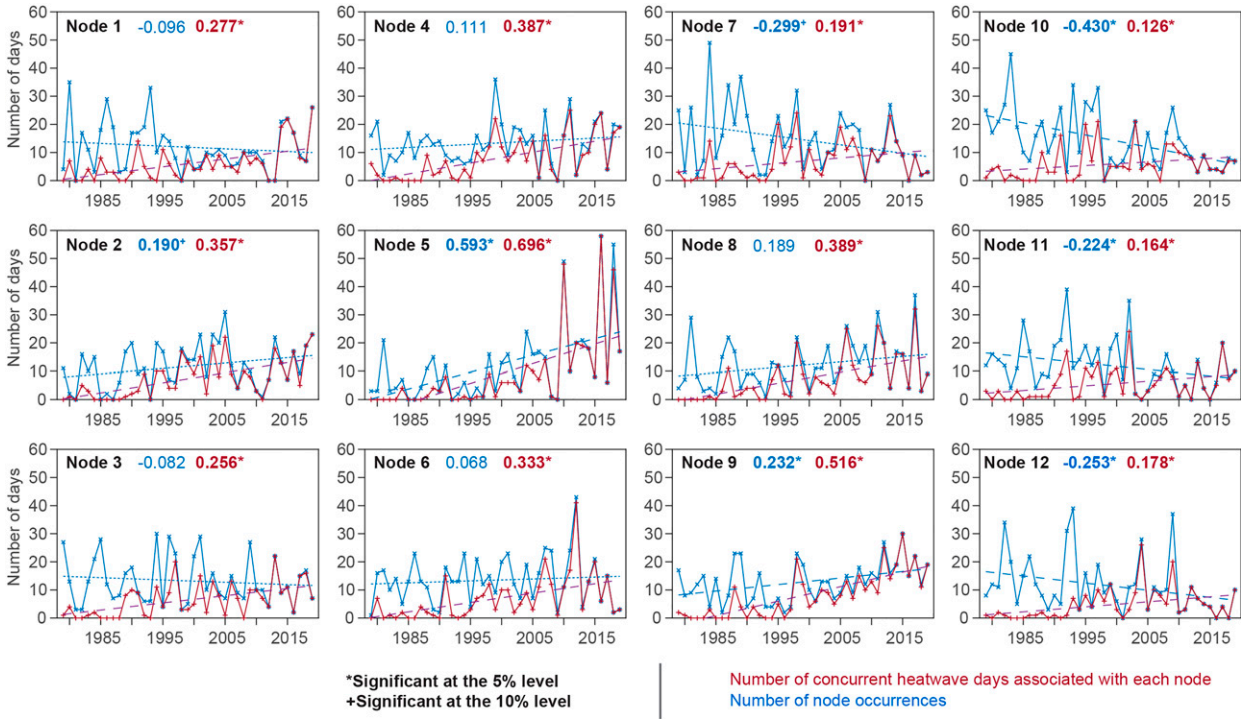

FIG. 6. Node and concurrent heatwave day frequencies. Subplots show the number of days that each node occurs (blue lines with "×" markers; left axis), the number of concurrent heatwave days per MJJAS season (red lines with "+" markers; left axis). Dashed blue (red) lines and bolded statistics with asterisks above subplots show that trends in the number of node occurrences (number of concurrent heatwave days) are significant at the 95% confidence level using the Mann–Kendall test. Bolded statistics with "+" markers show that trends are significant at the 90% confidence level. Decadal trends for these metrics are given in Table 1 and at the top of each subplot. Dotted lines show trends that are not significant at the 95% confidence level.

also exist outside this region (Fig. 5). For example, node 5 shows a high chance of concurrent heatwaves over the Barents and Kara Seas (Fig. 5). This suggests that midlatitude circulation patterns have teleconnections with heatwaves in regions outside the midlatitudes.

c. *Changes in large-scale atmospheric circulation patterns*

To examine how changes in circulation patterns may have influenced changes in spatial patterns of concurrent heatwaves, we examine trends in the frequency of each node and their associated concurrent heatwave days (Fig. 6 and Table 1). Changes in circulation patterns are likely to affect trends in concurrent heatwave day frequency and heatwave location. The occurrence of circulation patterns represented by nodes 5 and 9 increased significantly by 0.59 and 0.23 days per season, respectively, between 1979 and 2019, whereas patterns represented by nodes 10, 11, and 12 decreased significantly by between 0.22 and 0.43 days per season at the 95% confidence level (Fig. 6 and Table 1). Node 2 (node 7) also shows a significant increase (decrease) in frequency at the 90% confidence level. Concurrent heatwave day trends were significantly positive for all nodes at the 95% confidence level (Fig. 6 and Table 1). These trends were strongest for the nodes with significantly increasing frequencies—nodes 5 (0.70 days per season) and 9 (0.52 days per season)—and weakest for the nodes with significantly decreasing frequencies, nodes 10, 11, and 12.

While the increase in concurrent heatwave days associated with most nodes points to the influence of warming (Fig. 6), the disproportionate increase in concurrent heatwave days associated with certain nodes underscores the importance of dynamic changes in specific concurrent heatwave configurations. The increase in concurrent heatwave day trends for node 9 is approximately twice as large as the trend in node occurrence, whereas for node 5 it is only 1.2 times greater than the node occurrence trend (Table 1). A similar trend in node 5 frequency and concurrent heatwave days suggests a relatively large dynamic contribution in increases in the pattern of concurrent heatwaves associated with node 5 (Table 1). Differences between node frequency and concurrent heatwave frequency trends emphasize the interactions between the pattern of mean warming and circulation changes in driving the overall pattern of concurrent heatwave trends.

d. *Relative contribution of changing circulation patterns and warming*

We use a methodology similar to Cassano et al. (2007) and Horton et al. (2015) to decompose the total trend in concurrent heatwave days for each node into the thermodynamic, dynamic, and interactive term contributions (Table 1; see section 3 for details). We consider the dynamic contribution as a percentage of the thermodynamic contribution in order to

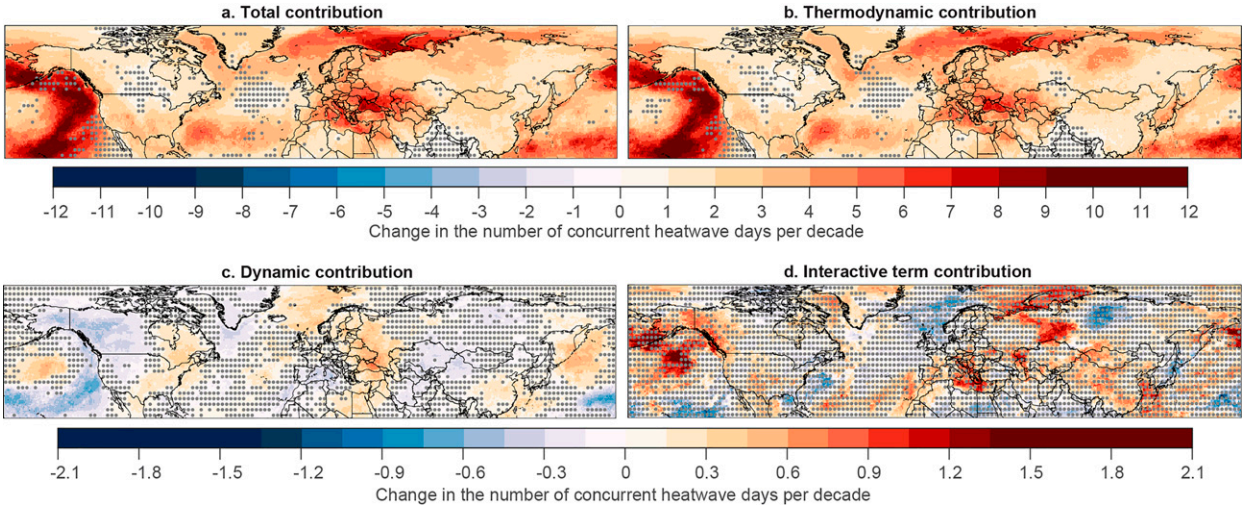

FIG. 7. Mechanistic drivers of concurrent heatwave trends. (a) The overall trend in the number of concurrent heatwave days per season (MJJAS), and the (b) thermodynamic (warming-driven), (c) dynamic (circulation-driven), and (d) interactive term contributions of this trend. The sum of these three contributions is equal to the total contribution in (a). Note that different color scales are used for the top and bottom rows, and the color scales are not linear at their tails. Stippling shows where trends are not significant. Significance is calculated using the Mann–Kendall test (Fatichi 2020) at the 95% confidence level.

examine the relative importance of changes in circulation to the effect of warming for each node (Table 1). The thermodynamic contribution to concurrent heatwave day trends is positive and larger than the dynamic contribution for all nodes (Table 1). In contrast, the sign of the dynamic contribution varies for different circulation patterns, with four of the 12 nodes (nodes 2, 5, 8, and 9) showing substantial positive contributions (>30%), implying that dynamical changes support the pattern of concurrent heatwaves associated with those nodes, and four nodes (nodes 7, 10, 11, and 12) showing substantial negative contributions (<−30%), implying that dynamical changes suppress the associated concurrent heatwave configurations.

Although relatively small for most nodes, the interactive term contributes 11% and 8% to the overall increase in concurrent heatwaves associated with nodes 5 and 9, respectively (not shown). The concurrent heatwave hotspots associated with nodes 5 and 9 (Fig. 5) coincide with several regions of high land–atmosphere feedbacks such as the eastern United States (Koster et al. 2006; Seneviratne et al. 2006) and central Europe (Seneviratne et al. 2006). An increasing trend in these interactions, suggested by the positive contribution of the interactive term, could indicate a strengthening of the land–atmosphere coupling. Another mechanism through which land surface interactions could affect concurrent heatwave occurrence is identified by Li et al. (2021), who note a relationship between heatwaves and various vegetation characteristics.

The decomposition of historical trends suggests that while concurrent heatwave days are increasing across the entire mid- to high latitudes largely due to mean warming, circulation and dynamic/thermodynamic interaction changes have also substantially contributed to the co-occurrence of heatwaves across the hotspots associated with the increasingly occurring circulation patterns (nodes 5 and 9). To examine the spatial variability of the influence of the different contributions, we quantify the thermodynamic, dynamic, and interactive term contributions (Figs. 7b, 7c, and 7d, respectively) to overall trends in concurrent heatwave days (Fig. 7a). The trend in the number of concurrent heatwave days at each grid cell shows the temporal change in the number of days that the cell is part of a concurrent heatwave.

The thermodynamic contribution (up to 11.8 concurrent heatwave days per decade) is much greater than the dynamic or interactive term contributions (up to 0.8 and 2.0 concurrent heatwave days per decade, respectively) over the majority of the region (Figs. 7b–d). Further, the interactive term is generally greater than the dynamic contribution alone, but is less significant (Figs. 7c,d). The strongest trends in concurrent heatwave days occur over regions including eastern Europe, the Barents and Kara Seas, and the eastern Pacific, where the thermodynamic contributions are strongest (Figs. 7a,b). These regions largely correspond to areas where mean warming is greatest (Fig. S2), except for the eastern Pacific. The dynamic and interactive term contributions exacerbate the trends over Europe and the Barents and Kara Seas (Figs. 7a,c,d). On the other hand, the dynamic contribution acts to dampen the trend over the eastern Pacific (Fig. 7c). The dynamic (interactive term) contribution also has relatively high positive values over eastern North America and the North Pacific (parts of Asia and the Pacific Ocean). Since these areas roughly correspond with where the thermodynamic contributions are relatively low (Fig. 7b), concurrent heatwaves in these regions are relatively more strongly affected by the circulation terms than those in other regions. Therefore, our results demonstrate that while the number of concurrent heatwaves across the Northern Hemisphere mid- to high latitudes is increasing (Fig. 2), some locations see a greater increase in these events than others

(Fig. 7a). Further, some of the regions with significant increases in concurrent heatwaves (Fig. 7a) correspond to concurrent heatwave hotspots in nodes with increasing frequency (nodes 5 and 9; Fig. 5). This indicates that dynamically driven concurrent heatwave changes during nodes 5 and 9 (Fig. 7c) compound and amplify thermodynamically driven changes (Fig. 7b).

We note two key caveats of our trend decomposition analyses. First, the decomposition technique used in this paper identifies the dynamic contribution specifically as the changes in the frequency of specific circulation patterns, assuming the patterns are stationary. However, geopotential height anomalies have increased significantly between 1979–98 and 2000–19 (Figs. S3 and S6a) and these increases are nonuniform, affecting the pattern of the anomalies in the various nodes. These within-node changes are not accounted for by the decomposition method used to identify dynamic trends. Although this could result in an underestimation of the role of dynamics to drive concurrent heatwaves, the influence of within-node changes is likely small over the 41 years of analysis, relative to the more substantial changes identified in Gervais et al. (2020) and Hassanzadeh et al. (2020) that identify changes on century time scales with much more warming. Further, by analyzing trends in circulation patterns using 12 stationary nodes (Fig. 4), our analysis is unlikely to consider potential changes in the waviness of the midlatitude circulation, as examined in Cattiaux et al. (2016). However, there is no significant trend in historical (1979–2014) waviness over the Northern Hemisphere in summer and only limited changes over certain regions (Cattiaux et al. 2016).

Second, the decomposition specifically aims to examine the contributions of mean temperature increases and changes in circulation patterns to concurrent heatwave trends. However, the spatial pattern of warming affects geopotential heights and could affect the circulation patterns and their changes. To evaluate the influence of the zonally asymmetric pattern of warming on geopotential height, we test the sensitivity of our results by comparing SOMs created using raw and detrended geopotential height data, where data are detrended by removing the zonal mean trend for each latitude, thus accounting for the amplified warming in the Arctic. Despite removing the zonal mean trend, we still find significant trends in some, albeit fewer, circulation patterns (node 9 has a significant positive trend and node 10 has a significant negative trend; not shown), showing that the changes in circulation patterns are not solely driven by zonally asymmetric mean warming (see section S3 in the online supplemental material). However, differences in the circulation pattern changes derived from the raw and detrended geopotential height data suggest that the spatial pattern of historical geopotential height changes could be influencing midlatitude circulation patterns. Although we have chosen to use the observed raw geopotential heights for our analysis that are an outcome of natural variability, feedbacks, and thermodynamic warming within the climate system, the influence of warming on historical circulation changes warrants further investigation.

While this paper identifies changes in circulation patterns in the midlatitudes that contribute to increasing risk of concurrent large heatwaves, the causes of change in midlatitude circulation patterns are an active research area with several potential mechanisms proposed in the literature (Cohen et al. 2020). Amplified land warming in the high latitudes can provide favorable conditions for waveguide formation and quasi-resonant amplification (Mann et al. 2017; Mann et al. 2018), while increasingly dry soils in the midlatitudes have been suggested as Rossby wave sources (Teng and Branstator 2019). Dynamical processes, such as eddy kinetic energy (Coumou et al. 2015), diabatic heating, and transient momentum fluxes (Ma and Franzke 2021), are shown to influence heatwaves in the Northern Hemisphere midlatitudes, with Coumou et al. (2015) identifying a weakening of summer eddy kinetic energy as a potential driver of increased heatwave persistence. In addition, anomalous heating in the tropical Atlantic has been associated with European heatwaves (Cassou et al. 2005), and the cooling of the Subpolar Gyre, potentially due to the Atlantic meridional overturning circulation slowdown (Caesar et al. 2018), can impose a ridge–trough pattern over the Atlantic Ocean and also lead to circulation changes (Duchez et al. 2016). Changing meridional temperature gradients due to uneven rates of global warming, such as Arctic amplification, have been suggested to slow down the midlatitude circulation (Kornhuber and Tamarin-Brodsky 2021) and could affect the frequency or amplitude of certain circulation patterns (e.g., Coumou et al. 2018, 2015; Zhang et al. 2020; Kornhuber et al. 2019). Investigating the influence of sea surface temperatures, sea ice conditions, and external forcings on the circulation patterns identified in our analysis could help isolate the causes of these changes (Wolf et al. 2020).

Attributing historical circulation changes requires model simulations to isolate the effect of natural variability from forced climate change. Analyzing trends in long preindustrial climate simulations, or model simulations of the "counterfactual" world without anthropogenic global warming, could provide a better understanding of the relative influences of internal variability and mean warming on circulation patterns and concurrent heatwaves. The significance in circulation pattern changes from 1979 to 2019 despite removing the mean increase in geopotential heights (see section S3 in the online supplemental material) suggests a considerable influence of natural variability in driving changes in circulation pattern frequencies and concurrent heatwave locations. Common natural modes of climate variability are known to affect heatwaves in certain locations. For example, Zhou and Wu (2016) identify a relationship between European heatwaves and El Niño–Southern Oscillation (ENSO) and the Atlantic multidecadal oscillation, and Wei et al. (2020) identify a link between heatwaves in China and ENSO and the Indian Ocean dipole. The strong trends observed over the northeast Pacific (Fig. 7) could indicate an influence from the Pacific decadal oscillation on concurrent heatwave frequency over this region, but this has not been investigated in this paper.

While previous work has largely focused on regional-scale heatwaves, our work identifies the patterns of concurrent heatwaves across the hemisphere and their associated circulation changes. Overall, our analyses demonstrate that hemispheric-scale atmospheric patterns can cause simultaneous heatwaves across multiple hotspot regions in the mid- to high latitudes. This linkage has been demonstrated by other

researchers for rare events with specific characteristics (Kornhuber et al. 2020, 2019; Röthlisberger et al. 2019). The ability of different methodologies to identify connected heatwave regions highlights the complexity of these events. While some methods are appropriate for examining rare extreme events (e.g., Kornhuber et al. 2020), our methodology is unique in its ability to classify all days and configurations of concurrent heatwaves. For example, Kornhuber et al. (2020) examine concurrent heatwave regions in the Northern Hemisphere related to the occurrence of wavenumber-7 circulation patterns. These rare events are a subset of circulation patterns captured in our SOM and are classified predominately in nodes 2, 3, 9, and 10 (see Table S1 in the online supplemental material). The locations of concurrent heatwave hotspots associated with these nodes (Fig. 5) show similarities to regions with anomalously high surface air temperature for wave-7 events [central/eastern North America, western Europe, and western Asia; see Fig. 2d in Kornhuber et al. (2020)]. However, our results with SOMs are not directly comparable to those in Kornhuber et al. (2020) due to three main reasons. First is the difference in methodologies and definitions: while we examine circulation patterns between 30° and 60°N that persist for 3 days, Kornhuber et al. (2020) examine circulation patterns between 37.5° and 57.5°N that persist for 7 days. Second, SOMs use all data in a sample to identify commonly occurring features, whereas by selectively analyzing wave-7 events Kornhuber et al. (2020) exclusively examine rare events. And third, our analyses examine heatwaves over MJJAS, whereas Kornhuber et al. (2020) examine June–August heatwaves.

We show that changes in specific circulation patterns and their interactions with thermodynamics have contributed substantially to the observed increase in specific concurrent heatwave patterns (Table 1). These results emphasize the importance of constraining dynamical changes and dynamic/thermodynamic interactions, such as via feedbacks, to more accurately understand changes in concurrent heatwave risks. Consistent with Horton et al. (2015), we identify changes in midlatitude atmospheric patterns (Fig. 6) and our findings underscore the importance of dynamics in driving changes in temperature extremes over parts of the midlatitudes (Fig. 7c). While Horton et al. (2015) examined dynamic contributions to local-scale temperature extremes, by examining the mid- to high latitudes as a whole we identify the large-scale drivers that connect the occurrence of heat extremes in different regions and we leverage this interconnectedness of the climate system to identify signals in large-scale drivers that might otherwise be obscured by noise at finer scales. Although Vogel et al. (2020) found a negligible influence of dynamics on observed increases in individual heatwave magnitude, duration, and extent, their analyses did not differentiate the dynamic influences for certain circulation patterns or regions and instead considered the characteristics of the largest heatwaves over global land areas (Vogel et al. 2020). By aggregating across all land regions, their analysis obscures any potential influence of dynamics on heatwave changes at regional scales and might average over competing influences, as is demonstrated in our analysis. By examining various configurations of concurrent heatwaves across different regions (Fig. 5), our analysis can distinguish the influence of specific atmospheric circulation patterns (Fig. 4), despite the aggregate dynamic influence being small (Fig. 7). These regional differences are important when designing mitigation or adaptation strategies, assuming historical trends continue or accelerate. Further, by examining multiple circulation patterns we gain an understanding of which regions are simultaneously seeing an increase in the risk of heatwaves, which can have important implications for aid requirements, food production, or insurance payouts.

5. Summary and conclusions

Our research provides the first comprehensive examination of the trends and drivers of concurrent heatwaves across the Northern Hemisphere mid- to high latitudes. We find that over the past few decades, concurrent heatwave days (i.e., days when two or more large heatwaves occur simultaneously) have become more frequent, increasing from ~20 days per season in the 1980s to ~143 days per season in the 2010s (i.e., concurrent heatwaves occurred almost every day of MJJAS in the last decade). Concurrent heatwaves have also become larger, whereby the mean spatial extent increased by ~46%, and the hottest events have become hotter, where the maximum intensity increased by ~17%. Increases in concurrent heatwave day frequencies vary spatially, with the largest increases over eastern Europe, the Barents and Kara Seas, and the eastern Pacific. We find that changes in the midlatitude circulation patterns have significantly contributed to the spatial and temporal trends in concurrent heatwaves (an increase of up to 0.8 days per decade), despite the aggregate dynamic contribution to heatwave trends being small relative to the contribution of warming. Specifically, circulation patterns that are associated with concurrent heatwaves over eastern North America, Europe, eastern, western, and central Asia, northeastern Africa, the Barents and Kara Seas, the northeast Pacific, and the North Atlantic have increased by 2.3–5.9 days per decade over the observed record. Understanding the distinct contributions of these dynamic and thermodynamic factors can provide insights into the role of Earth system changes and natural variability that could amplify the risk of concurrent heatwaves in certain regions beyond what is expected with warming alone.

Historical warming is largely attributable to anthropogenic activities, and projected increases in greenhouse gas emissions are almost certainly going to enhance warming globally (IPCC 2013). However, the historical trends in midlatitude circulation patterns and the relative influence of forced and natural variability are still uncertain (Cohen et al. 2020, 2014; Coumou et al. 2018; Francis 2017; Francis et al. 2017) and pose challenges when projecting future circulation changes (Shepherd 2014). While the links between large-scale circulation and heat extremes (Coumou et al. 2018; Horton et al. 2015; Suarez-Gutierrez et al. 2020; Zhang et al. 2020) and concurrent heatwaves (Kornhuber et al. 2020, 2019; Röthlisberger et al. 2019) are well established, our paper demonstrates not only that changes in midlatitude circulation patterns are related to the changes in the number and location of concurrent heatwaves within the midlatitudes, but also that these relationships persist outside the region. The teleconnections between midlatitude circulation changes and concurrent

heatwaves in the mid- to high latitudes emphasize the importance of further investigating potential influences of remote regions, such as warming in the Arctic or tropics, on concurrent heatwave events, toward understanding how projected changes in these regions might influence concurrent heatwave risk across the Northern Hemisphere. Further, the contribution of dynamic/thermodynamic interactions in some regions highlights the importance of examining the role of feedbacks between the atmosphere and land surface and their changes (Fischer et al. 2007; Herold et al. 2016; Koster et al. 2006; Seneviratne et al. 2012, 2006).

Since heatwaves are hazardous to human populations and ecosystems (Hoegh-Guldberg et al. 2018; McKechnie et al. 2012; Sharpe et al. 2019; Xu et al. 2016), our work implies that past changes in circulation patterns have altered the vulnerability of various regions to concurrent heatwaves, disproportionately amplifying the risks over certain regions. Further research is needed to explore whether these circulation changes can be attributed to anthropogenic climate change or if they are a signal of multidecadal variability in the Earth system. The identification of regions that are at risk of experiencing heatwaves concurrently has implications for disaster management, food security, and other global networks. For example, multiple food producing regions being simultaneously compromised can have cascading impacts on global food availability and consequently prices, which can have negative consequences for food security (Gaupp et al. 2020; Kornhuber et al. 2020; Tigchelaar et al. 2018). In addition, multiple regions experiencing heatwave-related impacts such as wildfires, disruption of economic activity, and disruption of marine ecosystems that serve as sources of food and income for communities can also strain financial aid resources and the global economy. Our methodology and findings could be used in conjunction with future climate projections to examine how regional vulnerability and food security may be affected by future circulation changes and projected warming.

Acknowledgments. The authors thank Peter Gibson, Dmitri Kalashnikov, and Melissa Gervais for their insightful discussions about SOMs, which assisted in the development of this paper's methods. C.D.W.R. and D.S. are supported by Washington State University and the U.S. National Science Foundation through Grant AGS-1934383. K.K. is supported by the U.S. National Science Foundation through Grant AGS-1934358. S.E.P.-K. is supported by Australian Research Council Grant FT170100106. P.C.L. is supported by the U.S. National Science Foundation through Grant AGS-1621554. The majority of the analyses for this project were run on Washington State University's high-performance computing cluster, Kamiak. Data analyses are performed using Matlab, Python, and CDO. The following Matlab packages were utilized for our research: SOM Toolbox (Laboratory of Computer and Information Science 2009), the Climate Data Toolbox for Matlab (Greene et al. 2019), and the Mann–Kendall test package (Fatichi 2020). The authors declare no competing interests.

C.D.W.R. and D.S. conceived and designed the study with feedback from all authors. C.D.W.R. performed all analysis and lead the study. C.D.W.R. and D.S. wrote the paper with contributions from K.K., S.E.P.-K., and P.C.L.

Data availability statement. We acknowledge the use of ERA5 reanalysis as the key dataset used in the manuscript, which is accessible at https://cds.climate.copernicus.eu/cdsapp#!/search?type=dataset. The sources are provided in the Data section of the article (section 2).

REFERENCES

Australian Bureau of Meteorology, 2020: About the heatwave service. Accessed 18 June 2020, http://www.bom.gov.au/australia/heatwave/knowledge-centre/heatwave-service.shtml.

Barnes, E. A., and J. A. Screen, 2015: The impact of Arctic warming on the midlatitude jet-stream: Can it? Has it? Will it? *Wiley Interdiscip. Rev.: Climate Change*, **6**, 277–286, https://doi.org/10.1002/wcc.337.

Caesar, L., S. Rahmstorf, A. Robinson, G. Feulner, and V. Saba, 2018: Observed fingerprint of a weakening Atlantic Ocean overturning circulation. *Nature*, **556**, 191–196, https://doi.org/10.1038/s41586-018-0006-5.

Cassano, J. J., P. Uotila, A. H. Lynch, and E. N. Cassano, 2007: Predicted changes in synoptic forcing of net precipitation in large Arctic river basins during the 21st century. *J. Geophys. Res.*, **112**, G04S49, https://doi.org/10.1029/2006JG000332.

Cassou, C., L. Terray, and A. S. Phillips, 2005: Tropical Atlantic influence on European heat waves. *J. Climate*, **18**, 2805–2811, https://doi.org/10.1175/JCLI3506.1.

Cattiaux, J., Y. Peings, D. Saint-Martin, N. Trou-Kechout, and S. J. Vavrus, 2016: Sinuosity of midlatitude atmospheric flow in a warming world. *Geophys. Res. Lett.*, **43**, 8259–8268, https://doi.org/10.1002/2016GL070309.

Cohen, J., and Coauthors, 2014: Recent Arctic amplification and extreme mid-latitude weather. *Nat. Geosci.*, **7**, 627–637, https://doi.org/10.1038/ngeo2234.

——, and Coauthors, 2020: Divergent consensuses on Arctic amplification influence on midlatitude severe winter weather. *Nat. Climate Change*, **10**, 20–29, https://doi.org/10.1038/s41558-019-0662-y.

Collins, M., and Coauthors, 2013: Long-term climate change: Projections, commitments and irreversibility. *Climate Change 2013: The Physical Science Basis*, T. F. Stocker et al., Eds., Cambridge University Press, 1029–1136.

Copernicus Climate Change Service, 2021a: ERA5 hourly data on pressure levels from 1979 to present. Copernicus Climate Change Service (C3S) Climate Data Store (CDS), accessed 2021, https://cds.climate.copernicus.eu/cdsapp#!/dataset/reanalysis-era5-pressure-levels?tab=overview.

——, 2021b: ERA5 hourly data on single levels from 1979 to present. Copernicus Climate Change Service (C3S) Climate Data Store (CDS), accessed 2021, https://cds.climate.copernicus.eu/cdsapp#!/dataset/reanalysis-era5-single-levels?tab=overview.

Coumou, D., V. Petoukhov, S. Rahmstorf, S. Petri, and H. J. Schellnhuber, 2014: Quasi-resonant circulation regimes and hemispheric synchronization of extreme weather in boreal summer. *Proc. Natl. Acad. Sci. USA*, **111**, 12 331–12 336, https://doi.org/10.1073/pnas.1412797111.

——, J. Lehmann, J. Beckmann, 2015: The weakening summer circulation in the Northern Hemisphere mid-latitudes. *Science*, **348**, 324–327, https://doi.org/10.1126/science.1261768.

——, G. Di Capua, S. Vavrus, L. Wang, and S. Wang, 2018: The influence of Arctic amplification on mid-latitude summer

circulation. *Nat. Commun.*, **9**, 2959, https://doi.org/10.1038/s41467-018-05256-8.

Ding, Q., and B. Wang, 2005: Circumglobal teleconnection in the Northern Hemisphere summer. *J. Climate*, **18**, 3483–3505, https://doi.org/10.1175/JCLI3473.1.

Duchez, A., and Coauthors, 2016: Drivers of exceptionally cold North Atlantic Ocean temperatures and their link to the 2015 European heat wave. *Environ. Res. Lett.*, **11**, 074004, https://doi.org/10.1088/1748-9326/11/7/074004.

Fatichi, S., 2020: Mann-Kendall test. MATLAB Central File Exchange, accessed 30 September 2020, https://www.mathworks.com/matlabcentral/fileexchange/25531-mann-kendall-test.

Fischer, E. M., S. I. Seneviratne, P. L. Vidale, D. Lüthi, and C. Schär, 2007: Soil moisture–atmosphere interactions during the 2003 European summer heat wave. *J. Climate*, **20**, 5081–5099, https://doi.org/10.1175/JCLI4288.1.

Francis, J. A., 2017: Why are Arctic linkages to extreme weather still up in the air? *Bull. Amer. Meteor. Soc.*, **98**, 2551–2557, https://doi.org/10.1175/BAMS-D-17-0006.1.

——, S. J. Vavrus, and J. Cohen, 2017: Amplified Arctic warming and mid-latitude weather: New perspectives on emerging connections. *Wiley Interdiscip. Rev. Climate Change*, **8**, e74, https://doi.org/10.1002/wcc.474.

Ganguly, A. R., K. Steinhaeuser, D. J. Erickson, M. Branstetter, E. S. Parish, N. Singh, J. B. Drake, and L. Buja, 2009: Higher trends but larger uncertainty and geographic variability in 21st century temperature and heat waves. *Proc. Natl. Acad. Sci. USA*, **106**, 15 555–15 559, https://doi.org/10.1073/pnas.0904495106.

Gao, M., Y. Yang, H. Shi, and Z. Gao, 2019: SOM-based synoptic analysis of atmospheric circulation patterns and temperature anomalies in China. *Atmos. Res.*, **220**, 46–56, https://doi.org/10.1016/j.atmosres.2019.01.005.

Gaupp, F., J. Hall, S. Hochrainer-Stigler, and S. Dadson, 2020: Changing risks of simultaneous global breadbasket failure. *Nat. Climate Change*, **10**, 54–57, https://doi.org/10.1038/s41558-019-0600-z.

Gervais, M., J. Shaman, and Y. Kushnir, 2020: Impact of the North Atlantic warming hole on sensible weather. *J. Climate*, **33**, 4255–4271, https://doi.org/10.1175/JCLI-D-19-0636.1.

Gibson, P. B., P. Uotila, S. E. Perkins-Kirkpatrick, L. V. Alexander, and A. J. Pitman, 2016: Evaluating synoptic systems in the CMIP5 climate models over the Australian region. *Climate Dyn.*, **47**, 2235–2251, https://doi.org/10.1007/s00382-015-2961-y.

Greene, C. A., and Coauthors, 2019: The climate data toolbox for MATLAB. *Geochem. Geophys. Geosyst.*, **20**, 3774–3781, https://doi.org/10.1029/2019GC008392.

Hassanzadeh, P., C. Y. Lee, E. Nabizadeh, S. J. Camargo, D. Ma, and L. Y. Yeung, 2020: Effects of climate change on the movement of future landfalling Texas tropical cyclones. *Nat. Commun.*, **11**, 3319, https://doi.org/10.1038/s41467-020-17130-7.

Hennermann, K., 2020: ERA5: Data documentation. ECMWF, accessed 17 February 2020, https://confluence.ecmwf.int/display/CKB/ERA5%3A+data+documentation.

Herold, N., J. Kala, and L. V. Alexander, 2016: The influence of soil moisture deficits on Australian heatwaves. *Environ. Res. Lett.*, **11**, 064003, https://doi.org/10.1088/1748-9326/11/6/064003.

Hersbach, H., and Coauthors, 2019: Global reanalysis: Goodbye ERA-Interim, hello ERA5. *ECMWF Newsletter*, No. 159, ECMWF, Reading, United Kingdom, 17–24, https://www.ecmwf.int/node/19027.

Hoegh-Guldberg, O., and Coauthors, 2018: Impacts of 1.5°C global warming on natural and human systems. *Global Warming of 1.5°C*, V. Masson-Delmotte, Eds., IPCC, 175–311.

Horton, D. E., N. C. Johnson, D. Singh, D. L. Swain, B. Rajaratnam, and N. S. Diffenbaugh, 2015: Contribution of changes in atmospheric circulation patterns to extreme temperature trends. *Nature*, **522**, 465–469, https://doi.org/10.1038/nature14550.

IPCC, 2013: Summary for policymakers. *Climate Change 2013: The Physical Science Basis*, T. F. Stocker et al., Eds., Cambridge University Press, 1–29.

Jiang, N., K. Cheung, K. Luo, P. J. Beggs, and W. Zhou, 2012: On two different objective procedures for classifying synoptic weather types over east Australia. *Int. J. Climatol.*, **32**, 1475–1494, https://doi.org/10.1002/joc.2373.

——, K. Luo, P. J. Beggs, K. Cheung, and Y. Scorgie, 2015: Insights into the implementation of synoptic weather-type classification using self-organizing maps: An Australian case study. *Int. J. Climatol.*, **35**, 3471–3485, https://doi.org/10.1002/joc.4221.

Kohonen, T., 2014: *MATLAB Implementations and Applications of the Self-Organizing Map*. Unigrafia Oy, 201 pp.

Kornhuber, K., and T. Tamarin-Brodsky, 2021: Future changes in Northern Hemisphere summer weather persistence linked to projected Arctic warming. *Geophys. Res. Lett.*, **48**, https://doi.org/10.1029/2020GL091603.

——, S. Osprey, D. Coumou, S. Petri, V. Petoukhov, S. Rahmstorf, and L. Gray, 2019: Extreme weather events in early summer 2018 connected by a recurrent hemispheric wave-7 pattern. *Environ. Res. Lett.*, **14**, 054002, https://doi.org/10.1088/1748-9326/ab13bf.

——, D. Coumou, E. Vogel, C. Lesk, J. F. Donges, J. Lehmann, and R. M. Horton, 2020: Amplified Rossby waves enhance risk of concurrent heatwaves in major breadbasket regions. *Nat. Climamte Change*, **10**, 48–53, https://doi.org/10.1038/s41558-019-0637-z.

Koster, R. D., and Coauthors, 2006: GLACE: The Global Land–Atmosphere Coupling Experiment. Part I: Overview. *J. Hydrometeor.*, **7**, 590–610, https://doi.org/10.1175/JHM510.1.

Laboratory of Computer and Information Science, 2009: *SOM Toolbox*. Helsinki University of Technology, Laboratory of Computer and Information Science, accessed 2019, http://www.cis.hut.fi/projects/somtoolbox/.

Lee, M. H., S. Lee, H. J. Song, and C. H. Ho, 2017: The recent increase in the occurrence of a boreal summer teleconnection and its relationship with temperature extremes. *J. Climate*, **30**, 7493–7504, https://doi.org/10.1175/JCLI-D-16-0094.1.

Li, J., C. Y. Tam, A. P. K. Tai, and N. C. Lau, 2021: Vegetation–heatwave correlations and contrasting energy exchange responses of different vegetation types to summer heatwaves in the Northern Hemisphere during the 1982–2011 period. *Agric. For. Meteor.*, **296**, 108208, https://doi.org/10.1016/j.agrformet.2020.108208.

Liu, Y., R. H. Weisberg, and C. N. K. Mooers, 2006: Performance evaluation of the self-organizing map for feature extraction. *J. Geophys. Res.*, **111**, C05018, https://doi.org/10.1029/2005JC003117.

Loikith, P. C., and A. J. Broccoli, 2012: Characteristics of observed atmospheric circulation patterns associated with temperature extremes over North America. *J. Climate*, **25**, 7266–7281, https://doi.org/10.1175/JCLI-D-11-00709.1.

Lyon, B., A. G. Barnston, E. Coffel, and R. M. Horton, 2019: Projected increase in the spatial extent of contiguous US summer

heat waves and associated attributes. *Environ. Res. Lett.*, **14**, 114029, https://doi.org/10.1088/1748-9326/ab4b41.

Ma, Q., and C. L. E. Franzke, 2021: The role of transient eddies and diabatic heating in the maintenance of European heat waves: A nonlinear quasi-stationary wave perspective. *Climate Dyn.*, **56**, 2983–3002, https://doi.org/10.1007/s00382-021-05628-9.

Mann, M. E., S. Rahmstorf, K. Kornhuber, B. A. Steinman, S. K. Miller, and D. Coumou, 2017: Influence of anthropogenic climate change on planetary wave resonance and extreme weather events. *Sci. Rep.*, **7**, 45242, https://doi.org/10.1038/srep45242.

——, ——, ——, ——, ——, S. Petri, and D. Coumou, 2018: Projected changes in persistent extreme summer weather events: The role of quasi-resonant amplification. *Sci. Adv.*, **4**, eaat3272, https://doi.org/10.1126/sciadv.aat3272.

McEvoy, D., I. Ahmed, and J. Mullett, 2012: The impact of the 2009 heat wave on Melbourne's critical infrastructure. *Local Environ.*, **17**, 783–796, https://doi.org/10.1080/13549839.2012.678320.

McKechnie, A. E., P. A. R. Hockey, and B. O. Wolf, 2012: Feeling the heat: Australian landbirds and climate change. *Emu*, **112**, i–vii, https://doi.org/10.1071/MUv112n2_ED.

Meehl, G. A., and C. Tebaldi, 2004: More intense, more frequent, and longer lasting heat waves in the 21st century. *Science*, **305**, 994–997, https://doi.org/10.1126/science.1098704.

Mioduszewski, J. R., A. K. Rennermalm, A. Hammann, M. Tedesco, E. U. Noble, J. C. Stroeve, and T. L. Mote, 2016: Atmospheric drivers of Greenland surface melt revealed by self-organizing maps. *J. Geophys. Res. Atmos.*, **121**, 5095–5114, https://doi.org/10.1002/2015JD024550.

Nairn, J. R., and R. J. B. Fawcett, 2015: The excess heat factor: A metric for heatwave intensity and its use in classifying heatwave severity. *Int. J. Environ. Res. Public Health*, **12**, 227–253, https://doi.org/10.3390/ijerph120100227.

NASA, 2020: Global temperature. Global climate change–Vital signs of the planet, NASA, accessed 26 May 2020, https://climate.nasa.gov/vital-signs/global-temperature/.

Nicholls, N., C. Skinner, M. Loughnan, and N. Tapper, 2008: A simple heat alert system for Melbourne, Australia. *Int. J. Biometeor.*, **52**, 375–384, https://doi.org/10.1007/s00484-007-0132-5.

Perkins, S. E., 2015: A review on the scientific understanding of heatwaves—Their measurement, driving mechanisms, and changes at the global scale. *Atmos. Res.*, **164–165**, 242–267, https://doi.org/10.1016/j.atmosres.2015.05.014.

——, L. V. Alexander, and J. R. Nairn, 2012: Increasing frequency, intensity and duration of observed global heatwaves and warm spells. *Geophys. Res. Lett.*, **39**, L20714, https://doi.org/10.1029/2012GL053361.

Perkins-Kirkpatrick, S. E., and S. C. Lewis, 2020: Increasing trends in regional heatwaves. *Nat. Commun.*, **11**, 3357, https://doi.org/10.1038/s41467-020-16970-7.

Petoukhov, V., S. Petri, S. Rahmstorf, D. Coumou, K. Kornhuber, and H. J. Schellnhuber, 2016: Role of quasiresonant planetary wave dynamics in recent boreal spring-to-autumn extreme events. *Proc. Natl. Acad. Sci. USA*, **113**, 6862–6867, https://doi.org/10.1073/pnas.1606300113.

Pfahl, S., and H. Wernli, 2012: Quantifying the relevance of atmospheric blocking for co-located temperature extremes in the Northern Hemisphere on (sub-)daily time scales. *Geophys. Res. Lett.*, **39**, L12807, https://doi.org/10.1029/2012GL052261.

Pfleiderer, P., C. F. Schleussner, K. Kornhuber, and D. Coumou, 2019: Summer weather becomes more persistent in a 2°C world. *Nat. Climate Change*, **9**, 666–671, https://doi.org/10.1038/s41558-019-0555-0.

Raymond, C., and Coauthors, 2020: Understanding and managing connected extreme events. *Nat. Climate Change*, **10**, 611–621, https://doi.org/10.1038/s41558-020-0790-4.

Rebetez, M., O. Dupont, and M. Giroud, 2009: An analysis of the July 2006 heatwave extent in Europe compared to the record year of 2003. *Theor. Appl. Climatol.*, **95** (1–2), 1–7, https://doi.org/10.1007/s00704-007-0370-9.

Rogers, C. D. W., A. J. E. Gallant, and N. J. Tapper, 2019: Is the urban heat island exacerbated during heatwaves in southern Australian cities? *Theor. Appl. Climatol.*, **137**, 441–457, https://doi.org/10.1007/s00704-018-2599-x.

Röthlisberger, M., L. Frossard, L. F. Bosart, D. Keyser, and O. Martius, 2019: Recurrent synoptic-scale Rossby wave patterns and their effect on the persistence of cold and hot spells. *J. Climate*, **32**, 3207–3226, https://doi.org/10.1175/JCLI-D-18-0664.1.

Screen, J. A., and I. Simmonds, 2014: Amplified mid-latitude planetary waves favour particular regional weather extremes. *Nat. Climate Change*, **4**, 704–709, https://doi.org/10.1038/nclimate2271.

Seneviratne, S. I., D. Lüthi, M. Litschi, and C. Schär, 2006: Land–atmosphere coupling and climate change in Europe. *Nature*, **443**, 205–209, https://doi.org/10.1038/nature05095.

——, and Coauthors, 2012: Changes in climate extremes and their impacts on the natural physical environment. *Managing the Risks of Extreme Events and Disasters to Advance Climate Change Adaptation*, C. B. Field, Eds., Cambridge University Press, 109–230, https://doi.org/10.2134/jeq2008.0015br.

Sharpe, L., B. Cale, and J. L. Gardner, 2019: Weighing the cost: The impact of serial heatwaves on body mass in a small Australian passerine. *J. Avian Biol.*, **50**, e02355, https://doi.org/10.1111/jav.02355.

Shepherd, T. G., 2014: Atmospheric circulation as a source of uncertainty in climate change projections. *Nat. Geosci.*, **7**, 703–708, https://doi.org/10.1038/ngeo2253.

Singh, D., D. L. Swain, J. S. Mankin, D. E. Horton, L. N. Thomas, B. Rajaratnam, and N. S. Diffenbaugh, 2016: Recent amplification of the North American winter temperature dipole. *J. Geophys. Res. Atmos.*, **121**, 9911–9928, https://doi.org/10.1002/2016JD025116.

Suarez-Gutierrez, L., W. A. Müller, C. Li, and J. Marotzke, 2020: Dynamical and thermodynamical drivers of variability in European summer heat extremes. *Climate Dyn.*, **54**, 4351–4366, https://doi.org/10.1007/s00382-020-05233-2.

Sui, C., L. Yu, and T. Vihma, 2020: Occurrence and drivers of wintertime temperature extremes in Northern Europe during 1979–2016. *Tellus*, **72A**, 1788368, https://doi.org/10.1080/16000870.2020.1788368.

Swiss Re, 2019a: Natural catastrophes and man-made disasters in 2018: "Secondary" perils on the frontline. *Sigma*, 2, 36 pp., https://www.swissre.com/dam/jcr:c37eb0e4-c0b9-4a9f-9954-3d0bb4339bfd/sigma2_2019_en.pdf.

——, 2019b: Insurance in a world of climate extremes: What latest science tells us. Swiss Re, 8 pp., https://www.swissre.com/dam/jcr:f2ec0485-5732-4204-9a67-e754978fedbc/Insurance_climate_extremes_expertise_publication.pdf.

Tan, X., S. Chen, T. Y. Gan, B. Liu, and X. Chen, 2019a: Dynamic and thermodynamic changes conducive to the increased occurrence of extreme spring fire weather over western Canada under possible anthropogenic climate change. *Agric. For. Meteor.*, **265**, 269–279, https://doi.org/10.1016/j.agrformet.2018.11.026.

——, T. Y. Gan, S. Chen, D. E. Horton, X. Chen, B. Liu, and K. Lin, 2019b: Trends in persistent seasonal-scale atmospheric circulation patterns responsible for seasonal precipitation totals and occurrences of precipitation extremes over Canada. *J. Climate*, **32**, 7105–7126, https://doi.org/10.1175/JCLI-D-18-0408.1.

Teng, H., and G. Branstator, 2019: Amplification of waveguide teleconnections in the boreal summer. *Curr. Climate Change Rep.*, **5**, 421–432, https://doi.org/10.1007/s40641-019-00150-x.

Thomas, C., A. Voulgarakis, G. Lim, J. Haigh, and P. Nowack, 2021: An unsupervised learning approach to identifying blocking events: the case of European summer. *Wea. Climate Dyn.*, **2**, 581–608, https://doi.org/10.5194/wcd-2-581-2021.

Tigchelaar, M., D. S. Battisti, R. L. Naylor, and D. K. Ray, 2018: Future warming increases probability of globally synchronized maize production shocks. *Proc. Natl. Acad. Sci. USA*, **115**, 6644–6649, https://doi.org/10.1073/pnas.1718031115.

van der Velde, M., G. Wriedt, and F. Bouraoui, 2010: Estimating irrigation use and effects on maize yield during the 2003 heatwave in France. *Agric. Ecosyst. Environ.*, **135**, 90–97, https://doi.org/10.1016/j.agee.2009.08.017.

Vesanto, J., J. Himberg, E. Alhoniemi, and J. Parhankangas, 2000: SOM toolbox for Matlab 5. Tech. Rep. **A57**, 2 pp.

Vogel, M. M., J. Zscheischler, R. Wartenburger, D. Dee, and S. I. Seneviratne, 2019: Concurrent 2018 hot extremes across Northern Hemisphere due to human-induced climate change. *Earth's Future*, **7**, 692–703, https://doi.org/10.1029/2019EF001189.

——, ——, E. M. Fischer, and S. I. Seneviratne, 2020: Development of future heatwaves for different hazard thresholds. *J. Geophys. Res. Atmos.*, **125**, https://doi.org/10.1029/2019JD032070.

Webb, L., J. Whiting, A. Watt, T. Hill, F. Wigg, G. Dunn, S. Needs, and E. W. R. Barlow, 2010: Managing grapevines through severe heat: A survey of growers after the 2009 summer heatwave in south-eastern Australia. *J. Wine Res.*, **21**, 147–165, https://doi.org/10.1080/09571264.2010.530106.

Wehrli, K., M. Hauser, and S. I. Seneviratne, 2020: Storylines of the 2018 Northern Hemisphere heatwave at pre-industrial and higher global warming levels. *Earth Syst. Dyn.*, **11**, 855–873, https://doi.org/10.5194/esd-11-855-2020.

Wei, J., W. Wang, Q. Shao, Z. Yu, Z. Chen, Y. Huang, and W. Xing, 2020: Heat wave variations across China tied to global SST modes. *J. Geophys. Res. Atmos.*, **125**, e2019JD031612, https://doi.org/10.1029/2019JD031612.

Wolf, G., A. Czaja, D. J. Brayshaw, and N. P. Klingaman, 2020: Connection between sea surface anomalies and atmospheric quasi-stationary waves. *J. Climate*, **33**, 201–212, https://doi.org/10.1175/JCLI-D-18-0751.1.

World Meteorological Organization, 2011: Weather extremes in a changing climate: Hindsight on foresight. WMO 1075, 16 pp., https://library.wmo.int/?lvl=notice_display&id=4132.

——, 2021: Updated 30-year reference period reflects changing climate. Accessed 7 May 2021, https://public.wmo.int/en/media/news/updated-30-year-reference-period-reflects-changing-climate.

Wu, B., and J. A. Francis, 2019: Summer Arctic cold anomaly dynamically linked to East Asian heat waves. *J. Climate*, **32**, 1137–1150, https://doi.org/10.1175/JCLI-D-18-0370.1.

Xu, Z., G. FitzGerald, Y. Guo, B. Jalaludin, and S. Tong, 2016: Impact of heatwave on mortality under different heatwave definitions: A systematic review and meta-analysis. *Environ. Int.*, **89–90**, 193–203, https://doi.org/10.1016/j.envint.2016.02.007.

Yu, L., Q. Yang, T. Vihma, S. Jagovkina, J. Liu, Q. Sun, and Y. Li, 2018: Features of extreme precipitation at Progress Station, Antarctica. *J. Climate*, **31**, 9087–9105, https://doi.org/10.1175/JCLI-D-18-0128.1.

Zhang, R., C. Sun, J. Zhu, R. Zhang, and W. Li, 2020: Increased European heat waves in recent decades in response to shrinking Arctic sea ice and Eurasian snow cover. *npj Climate Atmos. Sci.*, **3**, 7, https://doi.org/10.1038/s41612-020-0110-8.

Zhou, B., P. Zhai, and Y. Chen, 2020: Contribution of changes in synoptic-scale circulation patterns to the past summer precipitation regime shift in Eastern China. *Geophys. Res. Lett.*, **47**, e2020GL087728, https://doi.org/10.1029/2020GL087728.

Zhou, Y., and Z. Wu, 2016: Possible impacts of mega-El Niño/Southern Oscillation and Atlantic Multidecadal Oscillation on Eurasian heatwave frequency variability. *Quart. J. Roy. Meteor. Soc.*, **142**, 1647–1661, https://doi.org/10.1002/qj.2759.

Zscheischler, J., and Coauthors, 2018: Future climate risk from compound events. *Nat. Climate Change*, **8**, 469–477, https://doi.org/10.1038/s41558-018-0156-3.